Nanoscale Research Letters

NANO EXPRESS Open Access

Design, Modeling, and Fabrication of High-Speed VCSEL with Data Rate up to 50 Gb/s

Chih-Chiang Shen[1†], Tsung-Chi Hsu[1†], Yen-Wei Yeh[1], Chieh-Yu Kang[1], Yun-Ting Lu[1], Hon-Way Lin[1], Hsien-Yao Tseng[1], Yu-Tzu Chen[1], Cheng-Yuan Chen[1], Chien-Chung Lin[2], Chao-Hsin Wu[3], Po-Tsung Lee[1], Yang Sheng[4], Ching-Hsueh Chiu[1*] and Hao-Chung Kuo[1*]

Abstract

We have studied the characteristics of frequency response at 850-nm GaAs high-speed vertical-cavity surface-emitting lasers (VCSELs) with different kinds of oxide aperture sizes and cavity length using the PICS3D simulation program. Using 5-μm oxide aperture sizes, the frequency response behavior can be improved from 18.4 GHz and 15.5 GHz to 21.2 GHz and 19 GHz in a maximum of 3 dB at 25 °C and 85 °C, respectively. Numerical simulation results also suggest that the frequency response performances improved from 21.2 GHz and 19 GHz to 30.5 GHz and 24.5 GHz in a maximum of 3 dB at 25 °C and 85 °C due to the reduction of cavity length from 3λ/2 to λ/2. Consequently, the high-speed VCSEL devices were fabricated on a modified structure and exhibited 50-Gb/s data rate at 85 °C.

Keywords: High-speed VCSEL, PICS3D, 50 Gb/s, Oxide aperture, Cavity length

Introduction

In a few years, the vertical-cavity surface-emitting laser diodes (VCSELs) have become favorite transmitters for optical data links [1, 2]. Meanwhile, GaAs VCSEL devices have some advantages like low threshold current, power consumption, and small divergence angle, as well as top side illumination easily to make an array. Its demand has grown rapidly along with huge requirements for 5G Internet, 3D sensing, LiDAR, high-speed photodetectors, etc. [3–14].

PICS3D (Photonic Integrated Circuit Simulator in 3D) is a state-of-the-art 3D simulator for laser diodes and related active photonic devices. PISC3D is a 3D comprehensive numerical solver offering rigorous and self-consistent treatment on thermal, electrical, and optical properties by solving the related equations based on the nonlinear Newton-Raphson method. Its primary goal is to provide a 3D simulator for edge- and surface-emitting laser diodes. It has also been expanded to include models for other components integrated with or related to the laser emitter. In this study, we simulated GaAs VCSEL; of course, it also expanded easily to GaN VCSEL, LED, etc. [15, 16].

The first oxidation process in III–V compound material was discovered at the University of Illinois at Urbana-Champaign by Dallesasse and Holonyak in 1989 [17]. Through an oxidation process, the VCSEL devices can narrow down the size of oxide aperture diameter. Thus, it can not only promote a single transverse mode operation but also high-speed operation and single-mode performance.

To achieve a high modulation bandwidth, most designers would seek a large D-factor and reasonable low K-factor, typically a high differential gain by using strain QWs. A low photon lifetime by tuning the phase of the top distributed Bragg reflector (DBR) [18], a high confinement factor by employing a short cavity, and a small cavity oxide are necessary. On the other hand, reducing electrical parasitics can also improve modulation speed. These include parasitic capacitance from bond pads, intrinsic diode junction, and the area of out of aperture below metal contact pads which connects DBRs, oxidation layers, etc., and also include parasitic resistance from DBRs, junction resistance. However, parasitic

* Correspondence: jimchiu@nctu.edu.tw; hckuo.nctu@gmail.com
†Chih-Chiang Shen and Tsung-Chi Hsu contributed equally in this work.
[1]Department of Photonics & Graduate Institute of Electro-Optical Engineering, College of Electrical and Computer Engineering, National Chiao Tung University, Hsinchu 30010, Taiwan
Full list of author information is available at the end of the article

resistance is not better as low as possible; it needs to match 50 Ohm impedance. Regarding the high-speed VCSEL device development for data communication, there are several papers that record the progress [19, 20]. Today, the state-of-the-art 50-Gb/s 850-nm VCSEL devices have been demonstrated successfully at Chalmers University of Technology (CUT) by Westbergh et al. and University of Illinois Urbana-Champaign (UIUC) by Feng et al. [21–23]. We compared our experiments' result in this study with other labs, and our data is much close to their results.

However, the most effective way to increase the differential gain is the use of strain multiple quantum well (MQW), such as replacing the GaAs/AlGaAs MQW by the InGaAs/AlGaAs MQW [24, 25]. In the GaAs-based material, the hole effective mass is much larger than the electron effective mass, which causes the quasi-Fermi level to separate toward the valance band [26]. Hence, if we implement the strain on an active layer, the effective hole mass can be reduced significantly because the separation of the quasi-Fermi level is more balanced between the conduction and valance band. The differential gain can be considered as the growth of gain with carrier density once the quasi-Fermi level separation becomes more symmetric, and in the meanwhile, the differential gain will become more compressive in the strained MQW. Furthermore, the strain will also release the valance band mixing effect by increasing the energy difference between the heavy hole and light hole band. In this study, the numerical simulation was optimized to the VCSEL device structure through Crosslight PICS3D software [27].

Methods/experimental

Figure 1 shows the schematic of the 850-nm GaAs VCSEL device for simulation structure in this study. For this oxide VCSEL, the epitaxial layer structure from bottom to top includes a GaAs substrate, n-DBR of 34 pairs of $Al_{0.9}Ga_{0.1}As/Al_{0.12}Ga_{0.88}As$, an InGaAs MQW active layer with five $In_{0.08}Ga_{0.92}As$-strained QWs separated by six $Al_{0.37}Ga_{0.63}As$ quantum barrier layers, p-DBR, and a heavily doped p-GaAs as a contact layer. However, p-DBR layers include two $Al_{0.98}Ga_{0.02}As$ oxidation layers and four $Al_{0.96}Ga_{0.04}As$ oxidation layers and 13 pairs of $Al_{0.9}Ga_{0.1}As/Al_{0.12}Ga_{0.88}As$ layers. There are two kinds of oxide aperture sizes, 5 μm and 7 μm in our design. The two $Al_{0.98}Ga_{0.02}As$ oxidation layers would get an aperture confinement for the functions of electrical and optical, and the four $Al_{0.96}Ga_{0.04}As$ layers would reduce parasitic capacitance and further improve the optical response. Thus, we calculate the electrical potential and charge distribution via Poisson's equation, calculate carrier transport from the current continuity equations, use effective index method (EIM) approximation which has been successfully applied to calculate various VCSEL structures, and utilize the transfer-matrix method in the calculation of equivalent laser cavity. In this study, applied to perform our VCSEL simulations was the VCSEL modules in Crosslight PICS3D software which includes quantum mechanical, electrical, thermal, and DBR cavity optical effects, with stronger self-consistent interaction than any other optoelectronic devices that were applied to perform our VCSEL simulations. Considering that the simulated VCSEL structure is symmetric, cylindrical coordinate system, instead of the Cartesian coordinate system, was used for the sake of saving simulation time. The sophisticated Newton iteration formula was utilized in the software to ensure the correct answers to be found in nonlinear equations in the VCSEL module. In this report, we have especially considered different kinds of oxide aperture sizes and cavity lengths for improving VCSEL device performance. The VCSEL A and B are designed for 7-μm and 5-μm oxide aperture with 3λ/2 cavity length, respectively. On the other hand, VCSEL C adopts the design of 5-μm oxide aperture with λ/2 cavity length.

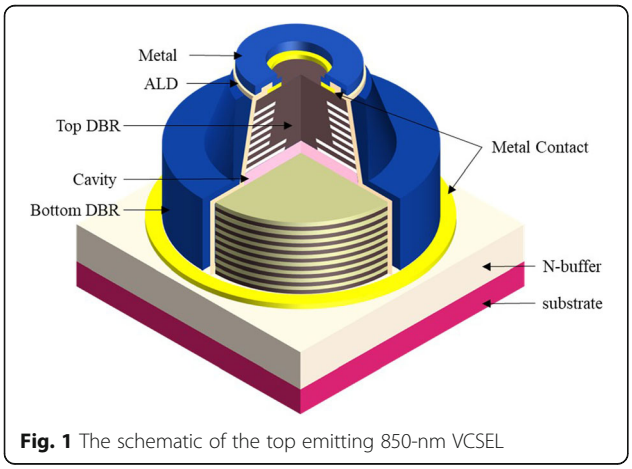

Fig. 1 The schematic of the top emitting 850-nm VCSEL

Results and Discussion

In VCSEL A and B, their cavity lengths are 3λ/2 but have different oxide aperture diameters 7 μm (VCSEL A) and 5 μm (VCSEL B), respectively. From simulation results, L-I curves are depicted in Fig. 2 a and b. We can see the threshold current of VCSEL B (I_{th} 0.6 mA and 0.73 mA) is always lower than the VCSEL A (I_{th} 0.82 mA and 0.94 mA) at 25 °C and 85 °C, respectively. Obviously, the I_{th} becomes bigger along with increasing oxide aperture size. To achieve the smallest possible mode-volume in the vertical direction and increase the D-factor, a short λ/2 optically thick cavity is used and then fixed at the 5-μm oxide aperture in VCSEL C. From the L-I curve, we can see the threshold current of VCSEL C (I_{th} 0.55 mA and 0.67 mA) are always lower than the VCSEL B (I_{th} 0.6 mA and 0.73 mA) at 25 °C and 85 °C, respectively, as shown in Fig. 3 a. In the experiment data of

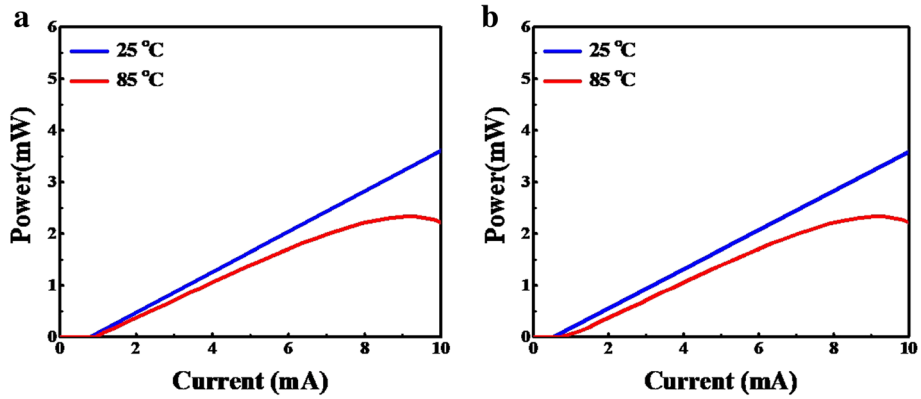

Fig. 2 The light-current characteristics for the simulation of VCSEL devices with 3λ/2 cavity length for **a** VCSEL A: 7 μm aperture diameter at 25 °C and at 85 °C, and **b** VCSEL B: 5 μm aperture diameter at 25 °C and at 85 °C

VCSEL C (real), L-I-V curves are shown in Fig. 3 b, the I_{th} of VCSEL C (real) are 0.8 mA and 1.08 mA at 25 °C and 85 °C, respectively. In the real case, because the thermal effect may induce the difference of I_{th} between the real case and simulation, results can be expected.

According to resonance frequency (*fr*) and damping rate function,

$$fr = D\cdot\sqrt{I-I_{\mathrm{th}}} \text{ where } D = \frac{1}{2\pi}\cdot\sqrt{\frac{\eta_i \Gamma V_g}{qV_a}\cdot\frac{\partial g}{\partial n}} \tag{1}$$

$$\gamma = K\cdot f_r{}^2 + \gamma_o \text{ where } K = 4\pi^2\left(\tau_p + \frac{\varepsilon}{v_g\left(\partial g / \partial n\right)}\right) \tag{2}$$

where D is the D-factor, I is the current, I_{th} is the threshold current, η_i is the internal quantum efficiency, Γ is the optical confinement factor, V_g is the group velocity, q is the elementary charge, V_a is the volume of the active (gain) region, $\frac{\partial g}{\partial n}$ is the differential gain, γ is the damping factor, K is the K-factor, γ_o is the damping factor offset, τ_p is the photon lifetime, and ε is the gain compression factor [28].

Thus, we can improve the frequency response of device performances by reducing the lifetime of photon and the effective volume of the resonator and increasing differential gain. Based on these considerations, we use the same parameters for the next section to improve the optical response. Figure 4 a–d shows the small-signal modulation response of VCSEL A and VCSEL B at 25 °C and 85 °C. From the simulation result of high-speed optical response, it has a good 3-dB bandwidth from 18.4 GHz and 15.5 G Hz (VCSEL A) to 21.2 GHz and 19 GHz (VCSEL B) and it also indicates the 3-dB bandwidth was enhanced by approximately 15.2% and 22.5%, respectively. Thus, attributed to the increasing confinement factor, the VCSEL devices have the lower threshold current in the emission and the batter bandwidth in VCSEL can be attributed to the confinement factor increased using smaller oxide aperture size.

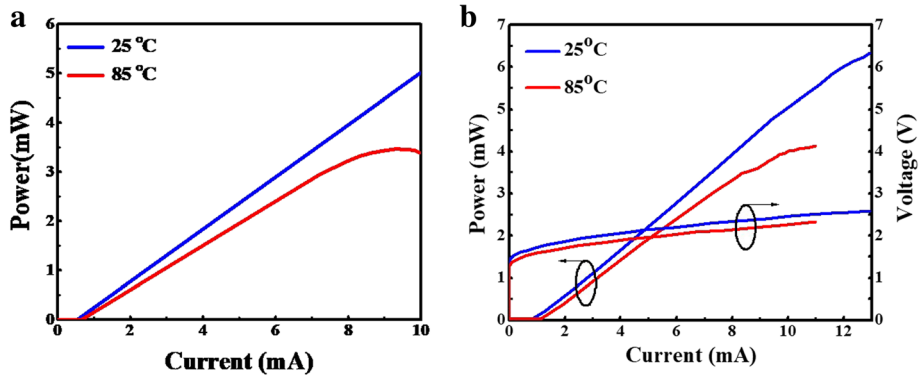

Fig. 3 a The light-current characteristics for the simulation of VCSEL C: λ/2 cavity length, 5 μm aperture diameter at 25 °C and 85 °C. **b** The measured light-current-voltage characteristics of VCSEL C at 25 °C and 85 °C

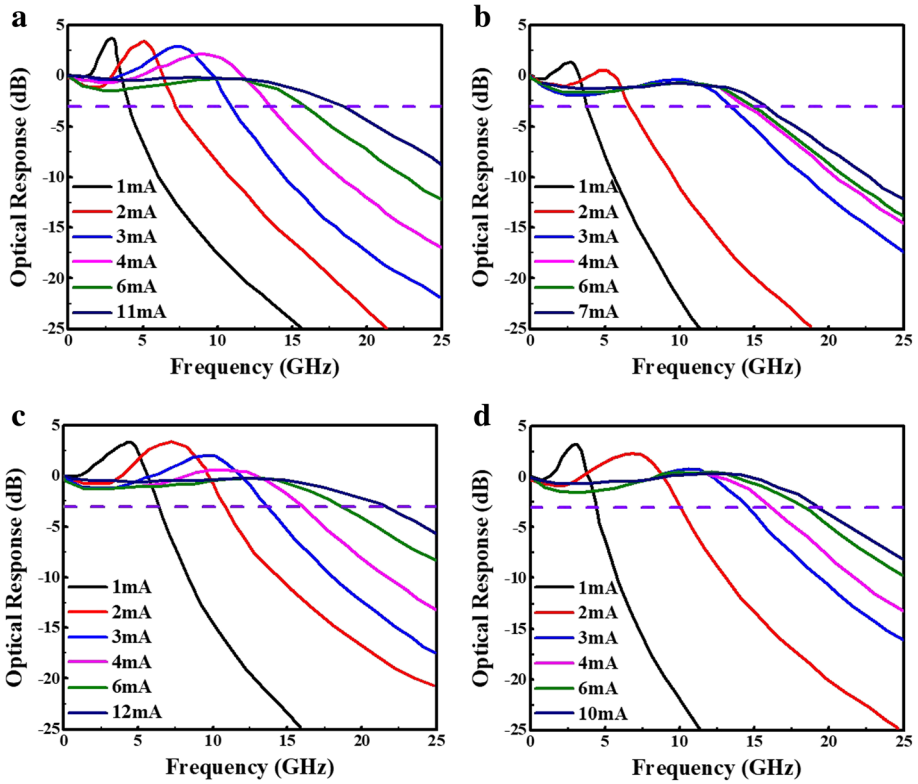

Fig. 4 Simulation of small-signal modulation response for VCSEL devices with 3λ/2 cavity length; thus, VCSEL A and B are with 7 μm and 5 μm aperture diameter, respectively, for VCSEL A at **a** 25 °C and at **b** 85 °C, and for VCSEL B at **c** 25 °C and at **d** 85 °C.

In the following case, we keep the 5-μm oxide aperture and shorten the cavity length to λ/2. Figure 5 a and b shows the small-signal modulation response of VCSEL C at 25 °C and 85 °C. From the simulation result of high-speed optical response, it has a good 3-dB bandwidth from 21.2 GHz and 19 GHz (VCSEL B) to 30.5 GHz and 24.5 GHz (VCSEL C) and it also indicates the 3-dB bandwidth was enhanced by approximately 43.9% and 28.9%, respectively. Thus, both simulation results show that the VCSEL devices which have the lower threshold current and larger bandwidth attributed to the increasing confinement factor using shorter cavity length.

Figure 6 shows simulated f3dB versus the square root of ($I - I_{th}$). The slope of these data points can be expressed as

$$f_{3dB} = D \times \sqrt{I - I_{th}} \quad (3)$$

The D-factor is an important parameter which related to internal quantum efficiency and the differential gain

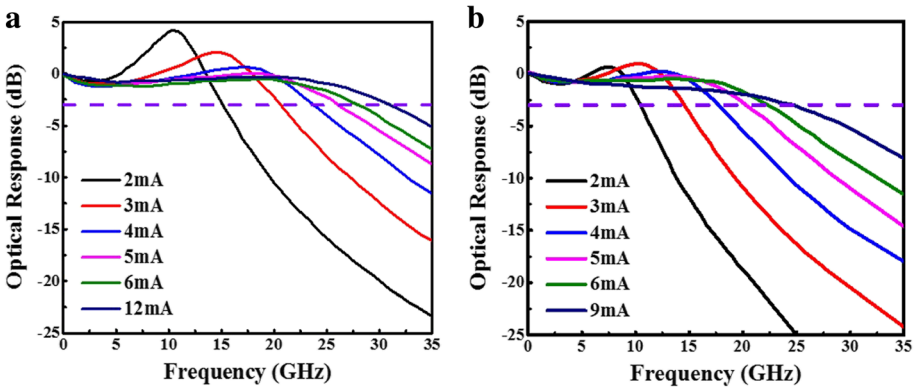

Fig. 5 Simulation of small-signal modulation response for VCSEL C: λ/2 cavity length, 5 μm aperture diameter at **a** 25 °C and at **b** 85 °C

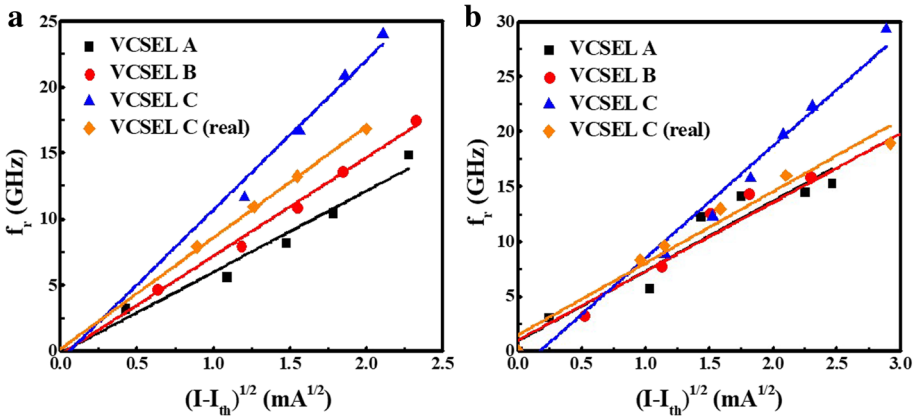

Fig. 6 The 3-dB frequency versus the square root of (I-I_{th}) of the simulation for VCSEL A,VCSEL B, VCSEL C, VCSEL C (real) at **a** 25 °C and **b** 85 °C

of the quantum wells for VCSEL operating at high speed [29]. Thus, the D-factor was 6.9, 7.3, and 11 GHz/$mA^{1/2}$ at 25 °C for VCSEL A, B, and C devices, respectively. On the other hand, the D-factor was 6.0, 6.7, and 9.4 GHz/$mA^{1/2}$ at 85 °C for VCSEL A, B, and C devices, respectively. From our results, the D-factor is inversely proportional to the oxide aperture diameter and cavity length. And the larger D-factor will be along with smaller threshold current. Furthermore, the VCSELs with smaller oxide aperture diameters (5 μm) and shorter cavity length (λ/2) are especially well-suited for data transmission at low energy per bit [30–32]. We expect the VCSEL can achieve error-free operation rate up to 50 Gb/s.

Next, we fabricated the VCSEL device and compared the simulation result and real test data; next, we fabricated the VCSEL device. In Fig. 6, the D-factor of VCSEL C (real) was 8.5 and 8.3 GHz/$mA^{1/2}$ at 25 °C and 85 °C, respectively. Figure 7 shows the measured small-signal modulation response at 25 °C and 85 °C. As we can see, the 3-dB bandwidth of measurement is 29.3 and 24.6 GHz at 25 °C and 85 °C, respectively. In the real device case, it was a little bit lower than the simulation case VCSEL C. The difference may come from the thermal effect and parasitic limitation due to device fabrication, as we mentioned earlier. Compared with others' results, our simulation is closer to our own experiments [21–23]. This points out that our VCSEL simulation result can be applied for the high-speed laser.

Conclusions

In conclusion, we optimized the oxide aperture and cavity length of the VCSEL structure by the PICS3D simulation program. Referring to these results, we fabricated 50-Gb/s VCSEL devices. The results showed a decrease in threshold current and improvement of 3-dB bandwidth in VCSEL devices. Finally, the high-speed VCSEL devices (up to 50-Gb/s data rate at 85 °C) had been demonstrated and successfully to create PICS3D model for 50-Gb/s VCSEL device design.

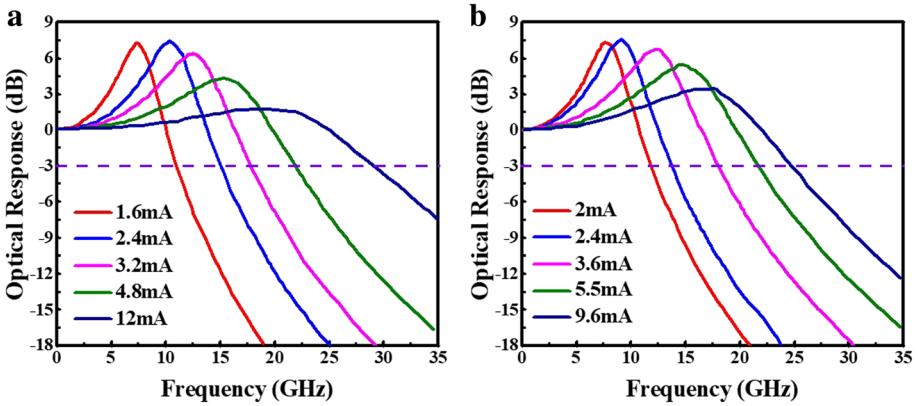

Fig. 7 Measured small-signal modulation response for VCSEL C (real): λ/2 cavity length, 5 μm aperture diameter at **a** 25 °C and **b** 85 °C

Abbreviations

EIM: Effective index method; MQW: Multiple quantum well; PICS3D: Photonic Integrated Circuit Simulator in 3D; QWs: Quantum wellsDBRDistributed Bragg reflector; VCSELs: Vertical-cavity surface-emitting lasers

Acknowledgements

We would like to thank Prof. Kenichi Iga and Prof. Fumio Koyama of Tokyo Institute of Technology, Prof. N. Holonyak Jr. and Prof. M. Feng of UIUC for giving us recommendations of high-speed VCSEL device physical models, Prof. C. Chang-Hasnain of UC Berkeley, and Prof. S. C. Wang and Prof. T. C. Lu of National Chiao Tung University to discuss the devices' structures, etc. Finally, we appreciate Crosslight for providing support of the simulation modeling tool.

Authors' Contributions

CCS, TCH, YWY, CYK, YTL, HWL, HYT, YTC, CHW, PTL, CCL, CHC, and HCK discussed the topic and experiments. YWY and YTL did the PICS3D simulations and consulted YS for the PICS3D tool. CHW manufactured and measured the devices. All authors discussed the data analysis and interpretation and contributed equally to the writing of the manuscript. All authors approved the final version of the manuscript.

Funding

The funding was supported by the Ministry of Science and Technology of Taiwan. The grant number is MOST 106-2218-E-005-001-.

Availability of Data and Materials

In the current work, the data and analysis are available from the corresponding authors on reasonable request.

Competing Interests

The authors declare that they have no competing interests.

Author details

[1]Department of Photonics & Graduate Institute of Electro-Optical Engineering, College of Electrical and Computer Engineering, National Chiao Tung University, Hsinchu 30010, Taiwan. [2]Institute of Photonic System, National Chiao Tung University, Tainan 71150, Taiwan. [3]Graduate Institute of Photonics and Optoelectronics, National Taiwan University, Taipei 10617, Taiwan. [4]Crosslight Software Inc., China Branch, Shanghai 200063, China.

Received: 21 May 2019 Accepted: 28 July 2019
Published online: 14 August 2019

References

1. Lu I-C, Wei C-C, Chen H-Y, Chen K-Z, Huang C-H, Chi K-L et al (2015) Very high bit-rate distance product using high-power single-mode 850-nm VCSEL with discrete multitone modulation formats through OM4 multimode fiber. IEEE Journal of Selected Topics in Quantum Electronics. 21(6):444–452
2. Mutig A, Bimberg D (2011) Progress on high-speed 980 nm VCSELs for short-reach optical interconnects. Advances in Optical Technologies. 2011
3. Cheng C-H, Shen C-C, Kao H-Y, Hsieh D-H, Wang H-Y, Yeh Y-W et al (2018) 850/940-nm VCSEL for optical communication and 3D sensing (From OEA, Vol. 1, No. 3). Opto-Electronic Review 2(03):a201903002
4. Michalzik R. VCSELs: fundamentals, technology and applications of vertical-cavity surface-emitting lasers: Springer; 2012.
5. Murty MR, Huang X, Liu G, Lin C, Xu D, Shieh C et al (2005) Long-wavelength VCSEL-based CWDM scheme for 10-GbE links. IEEE photonics technology letters. 17(6):1286–1288
6. Kao H-Y, Tsai C-T, Leong S-F, Peng C-Y, Chi Y-C, Wang H-Y et al (2018) Single-mode VCSEL for pre-emphasis PAM-4 transmission up to 64 Gbit/s over 100–300 m in OM4 MMF. Photonics Research 6(7):666–673
7. Kao H-Y, Chi Y-C, Tsai C-T, Leong S-F, Peng C-Y, Wang H-Y et al (2017) Few-mode VCSEL chip for 100-Gb/s transmission over 100 m multimode fiber. Photonics Research. 5(5):507–515
8. Shi J-W, Chen C-C, Wu Y-S, Guol S-H, Kuo C, Yang Y-J (2008) High-power and high-speed Zn-diffusion single fundamental-mode vertical-cavity surface-emitting lasers at 850-nm wavelength. IEEE Photonics Technology Letters 20(13):1121–1123
9. Wu W-L, Huang C-Y, Wang H-Y, Lin Y-H, Wu C-H, Kuo H-C, et al. VCSEL with bi-layer oxidized aperture enables 140-Gbit/s OFDM transmission over 100-m-long OM5 MMF. Optical Fiber Communication Conference; 2019: Optical Society of America.
10. Wang H-P, Periyanagounder D, Li A-C, He J-H (2018) Fabrication of silicon hierarchical structures for solar cell applications. IEEE Access. 7:19395–19400
11. Zhang Z, Ning Y, Fang X (2019) From nanofibers to ordered ZnO/NiO heterojunction arrays for self-powered and transparent UV photodetectors. Journal of Materials Chemistry C 7(2):223–229
12. Alamri AM, Leung S, Vaseem M, Shamim A, He J-H (2019) Fully inkjet-printed photodetector using a graphene/perovskite/graphene heterostructure. IEEE Transactions on Electron Devices. 66(6):2657–2661
13. Ning Y, Zhang Z, Teng F, Fang X (2018) Novel transparent and self-powered UV photodetector based on crossed ZnO nanofiber array homojunction. Small 14(13):1703754
14. Lin C-H, Cheng B, Li T-Y, JRnDn R, Wei T-C, Fu H-C et al (2018) Orthogonal lithography for halide perovskite optoelectronic nanodevices. ACS nano 13(2):1168–1176
15. Kou J, Shen C-C, Shao H, Che J, Hou X, Chu C et al (2019) Impact of the surface recombination on InGaN/GaN-based blue micro-light emitting diodes. Optics Express. 27(12):A643–AA53
16. Shen C-C, Lu Y-T, Yeh Y-W, Chen C-Y, Chen Y-T, Sher C-W et al (2019) Design and fabrication of the reliable gan based vertical-cavity surface-emitting laser via tunnel junction. Crystals 9(4):187
17. Dallesasse JM, Holonyak N Jr, Sugg A, Richard T, El-Zein N (1990) Hydrolyzation oxidation of Alx Ga_{1-x} As-AlAs-GaAs quantum well heterostructures and superlattices. Applied Physics Letters 57(26):2844–2846
18. Larsson A, Gustavsson JS, Westbergh P, Haglund E, Haglund EP, Simpanen E, et al., editors. VCSEL design and integration for high-capacity optical interconnects. Optical Interconnects XVII; 2017: International Society for Optics and Photonics.
19. Liu A, Wolf P, Lott JA, Bimberg D (2019) Vertical-cavity surface-emitting lasers for data communication and sensing. Photonics Research. 7(2):121–136
20. Westbergh P, Gustavsson JS, Kögel B, Haglund Å, Larsson A (2011) Impact of photon lifetime on high-speed VCSEL performance. IEEE Journal of Selected Topics in Quantum Electronics. 17(6):1603–1613
21. Westbergh P, Safaisini R, Haglund E, Gustavsson JS, Larsson A, Geen M et al (2013) High-speed oxide confined 850-nm VCSELs operating error-free at 40 Gb/s up to 85 °C. IEEE Photonics Technology Letters. 25(8):768–771
22. Liu M, Wang CY, Feng M, Holonyak N, editors. 850 nm oxide-confined VCSELs with 50 Gb/s error-free transmission operating up to 85 °C. CLEO: Science and Innovations; 2016: Optical Society of America.
23. Feng M, Wu C-H, Holonyak N (2018) Oxide-confined VCSELs for high-speed optical interconnects. IEEE Journal of Quantum Electronics. 54(3):1–15
24. Chan K, Li H, Chan C (1998) Optical gain of interdiffused InGaAs-As and AlGaAs-GaAs quantum wells. IEEE journal of quantum electronics. 34(1):157–165
25. O'Reilly EP, Adams AR (1994) Band-structure engineering in strained semiconductor lasers. IEEE Journal of Quantum electronics. 30(2):366–379
26. Coldren LA, Corzine SW, Mashanovitch ML (2012) Diode lasers and photonic integrated circuits. Hoboken: Wiley;
27. Crosslight PICS3D. Available: http://crosslight.com/products/pics3d/
28. O'Brien CJ, Majewski ML, Rakic AD (2007) A critical comparison of high-speed VCSEL characterization techniques. Journal of lightwave technology. 25(2):597–605
29. Healy SB, O'Reilly EP, Gustavsson JS, Westbergh P, Haglund Å, Larsson A et al (2010) Active region design for high-speed 850-nm VCSELs. IEEE Journal of Quantum Electronics. 46(4):506–512
30. Demeulenaere B, Bienstman P, Dhoedt B, Baets R (1999) Detailed study of AlAs-oxidized apertures in VCSEL cavities for optimized modal performance. IEEE journal of quantum electronics. 35(3):358–367
31. Larsson A, Westbergh P, Gustavsson J, Haglund Å, Kögel B (2010) High-speed VCSELs for short reach communication. Semiconductor Science and Technology. 26(1):014017
32. Haglund E, Westbergh P, Gustavsson JS, Haglund EP, Larsson A (2016) High-speed VCSELs with strong confinement of optical fields and carriers. Journal of Lightwave Technology. 34(2):269–277

Publisher's Note